Journal of Ovonic Research Vol. 18, No. 3, May - June 2022, p. 431 - 442

Effect of Au and Ag nanoparticles addition on the morphological, structural and optical properties of ZnO thin films deposited by sol-gel method

A. A. Kamil*, N. A. Bakr, T. H. Mubarak, J. Al-Zanganawee
Department of Physics, College of Science, University of Diyala, Diyala, Iraq

In the present study, ZnO thin films were deposited on quartz substrates by sol-gel spin-coating method. Zinc-diacetate (($Zn(CH_3COO)_2.2H_2O$), diolamine (DEA) ($HN(CH_2CH_2OH)_2$) and ethylene glycol monomethyl ether ($CH_3OCH_2CH_2OH$) were used as a precursor, stabilizer agent, and solvent, respectively. Au and Ag NPs were synthesized by (PLAL) technique using “Q-Switched ND-YAG laser” system with laser parameters (520 mJ laser energy, 1064 nm wavelength, 450 laser pulses, and 1Hz frequency). The volumetric ratios of ZnO source solution to Au and Ag colloidal solutions were 3:2 and 4:1, respectively. The morphological, structural and optical properties of ZnO thin films embedded with Au and Ag NPs were investigated. The patterns of x-ray diffraction (XRD) showed peaks indexed to (100), (002) and (101) planes for ZnO and (111), (200) and (220) for Au and Ag NPs. The surface morphology of the films was examined by FESEM and the Raman spectra of ZnO thin films embedded with Ag and Au NPs were investigated. Furthermore, the optical properties of the films were analyzed by UV-Vis spectroscopy measurements. The optical band gap of the films increased with increasing the volumetric ratios of ZnO embedded with Au and Ag NPs.

(Received February 10, 2022; Accepted June 6, 2022)

Keywords: Sol-gel spin coating, ZnO thin film, Structural properties, Au nanoparticles, Ag nanoparticles

1. Introduction

Zinc oxide (ZnO) was studied for several decades as an effective semiconductor. (ZnO) is non-toxic, abundant, low price compound with direct band gap (3.2–3.4 eV) [1–3]. Therefore, ZnO has huge different applications in optoelectronics devices due to its special electrical, optical, and crystal structural properties [4–6]. ZnO is an important multifunctional n-type semiconductor material. It has strong excitation binding energy (60 meV) [7]. ZnO has essential functional oxide, displaying high conductivity near the ultraviolet emission. ZnO is water-insoluble white powder, commonly can be used as an ingredient in many different products such as “glass, cement, lubricants, paints, ointments, foods, batteries, ferrites, fire retardants, and first aid tapes materials”. In addition, it has other high-tech applications such as photonic crystals, photodetectors, optical modulator waveguides, and solar cells. Properties of ZnO have been modified with many noble metals like (Pt, Au, Ag, Pd, etc). One of the important applications of ZnO films as active material in the gas sensing is due to its fast time response, short response/recovery time, and electrical performance [8].

Noble metal nanoparticles such as Ag and Au NPs have distinctive properties which make them useful for technological applications in physics, chemistry, biology, and medicine. Au and Ag NPs have very poor sensitivity to the physical factors such as air, light, and electronic characteristics. For instance, metal nanoparticles were employed in cancer radiation therapy [9], CT contrast agents [10], drug delivery [11], and sensors [12]. In the green and red regions of the UV-visible spectrum, Au NPs have a surface plasmon resonance effect as a result of the interaction of gold NPs conduction electrons with incident photons. In visible wavelength range, Au NPs are chemically stable and usually exhibit surface enhanced Raman scattering. The aim of this study is to investigate the effect of Au and Ag NPs addition on the morphological, structural and optical properties of ZnO thin films deposited by sol-gel process using spin coating method.

---

* Corresponding author: asaad181162@yahoo.com
https://doi.org/10.15251/JOR.2022.183.431

2. Experimental part

Zinc oxide thin films were prepared by sol-gel spin-coating method. Zinc acetate dihydrate ($Zn(CH_3COO)_2.2H_2O$) solution of 0.5 M molarity was prepared by dissolving 0.5487 g in 5 ml of ethylene glycol monomethyl ether ($CH_3OCH_2CH_2OH$) as solvent and di-ethanol-amine (DEA) as stabilizer. After stirring and heating at 60 ^oC for 60 min, clear homogeneous solution was obtained which is used to prepare the films. Au and Ag NPs were synthesized by (PLAL) technique using Q-switched (Nd:YAG) (HUAFEI, China) pulsed laser. The laser parameters (520 mJ laser energy 1064 nm wavelength, 450 laser pulses, and 1Hz frequency) were used in preparation of metal NPs. Pure Au and Ag metal targets were cleaned by 99.999% ethyl alcohol to remove any organic and dust materials from their surface. The targets were placed in a beaker filled with (5 ml) of Ethylene glycol monomethyl ether ($CH_3OCH_2CH_2OH$), and the distance between metals targets and laser lens was (60 mm) [13]. The volumetric ratios of ZnO source solution to Au and Ag colloidal solution were 3:2 and 4:1, respectively. For deposition of multilayers of Au and Ag embedded in ZnO nanostructure thin films by spin coating method, clean quartz glass substrate with dimensions of (2, 1.5, and 0.1 cm) was fixed onto the stage of spin coating system (Ossila, UK). The rotation disc speed was adjusted at 3000 rpm for 30 s. After each layer deposition, the sample was removed from the spin coating disc and dried on hotplate at 150 ^oC for 15 minutes in air. This process was repeated to make multilayer thin films. The thin films samples were annealed at 400 ^oC for 1 hour using muffle furnace. Figure (1) shows a schematic diagram of spin coating process. The microstructure and elemental analysis of the films were investigated by Field Emission Scanning Electron Microscopy (FESEM) and Energy Dispersive X-ray Spectroscopy (EDS) from (TESCAN MIRA3, Czech Republic), respectively. The films were characterized by Low Angel X-Ray Diffraction (TYPE: Bruker D8 Advance Machine, Germany) using CuKα wavelength at 40 kV and 30 mA. The absorption spectra of the samples were measured by UV/Vis spectrophotometer (UV-1800, Shimadzu, Japan).

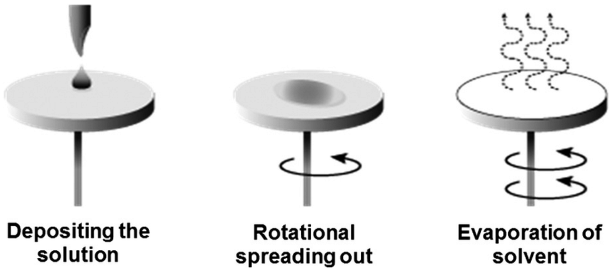

Fig. 1. A schematic diagram of spin coating process [14].

3. Results and discussion

3.1. Morphological analysis

3.1.1. FESEM analysis of pure ZnO embedded with Au and Ag NPs

The surface morphology of pure ZnO, ZnO+Au (3:2), ZnO+Au (4:1), ZnO+Ag (3:2), and ZnO+Ag (4:1) thin films deposited on a quartz substrate were examined by FESEM. Figure (2) illustrates the images at 50 KX magnification of pure zinc oxide ZnO (0.5 M) thin film deposited on quartz substrate. This figure shows that the surface morphology of the film is homogeneous with uniform distribution of ZnO nanostructures over the scanned area with cauliflower like shapes. The average of particle size of pure ZnO thin film was estimated by Image J software and found to be 36.6 nm.

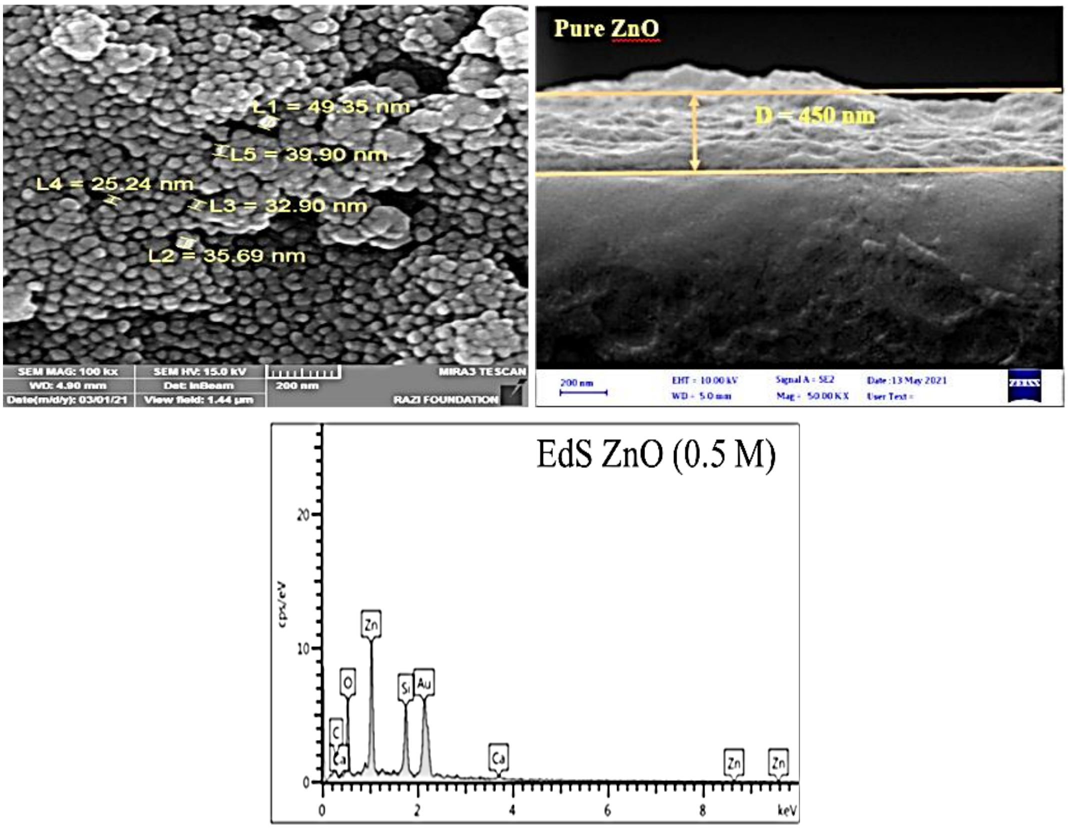

Fig. 2. FESEM images of (ZnO) (0.5 M) thin film.

Figure 3 illustrates the images at 50 KX magnification of ZnO+Au (3:2) thin film deposited on a quartz substrate. The surface morphology of thin films is homogeneous with uniform distribution of spherical shapes with an average size of 79.9 nm.

Figure 4 shows the images at 50 KX magnifications of ZnO+Au (4:1) thin film coated on a quartz substrate. The figure shows randomly scattered semi spherical particles with size-distribution of nanocrystallites and agglomeration takes place. From FESEM image, it is found that the average size of 69.61 nm particle diameter, which is in agreement with other reports [15]. EDS spectra shown in the figures (2, 3 and 4) confirm that all the elements of (Zn, O, Au) are present in the deposited samples. Strong interactions occur between the functional groups with Au coated on ZnO nanoparticles [16].

Figure 5 illustrates FESEM analysis of pure zinc oxide thin films embedded with silver NPs (a. (ZnO+Ag) (3:2) and b. (ZnO+Ag) (4:1)). In Figure 5 a, the images at 50 KX magnification exhibit almost cauliflower like shapes with irregular size-distribution nanocrystallites. ZnO+Ag (3:2) surface demonstrates grain size value of about 75.62 nm. Figure 5 b displays randomly scattered cauliflower particles of irregular size of ZnO+Ag (4:1). The value of grain size is about 68.02 nm. From the cross-section images, it can be noticed a change of the films thickness with the volumetric ratios. EDS spectra shown in figure 5 confirm that all the composition elements (Zn, O, Ag) are present in the deposited samples.

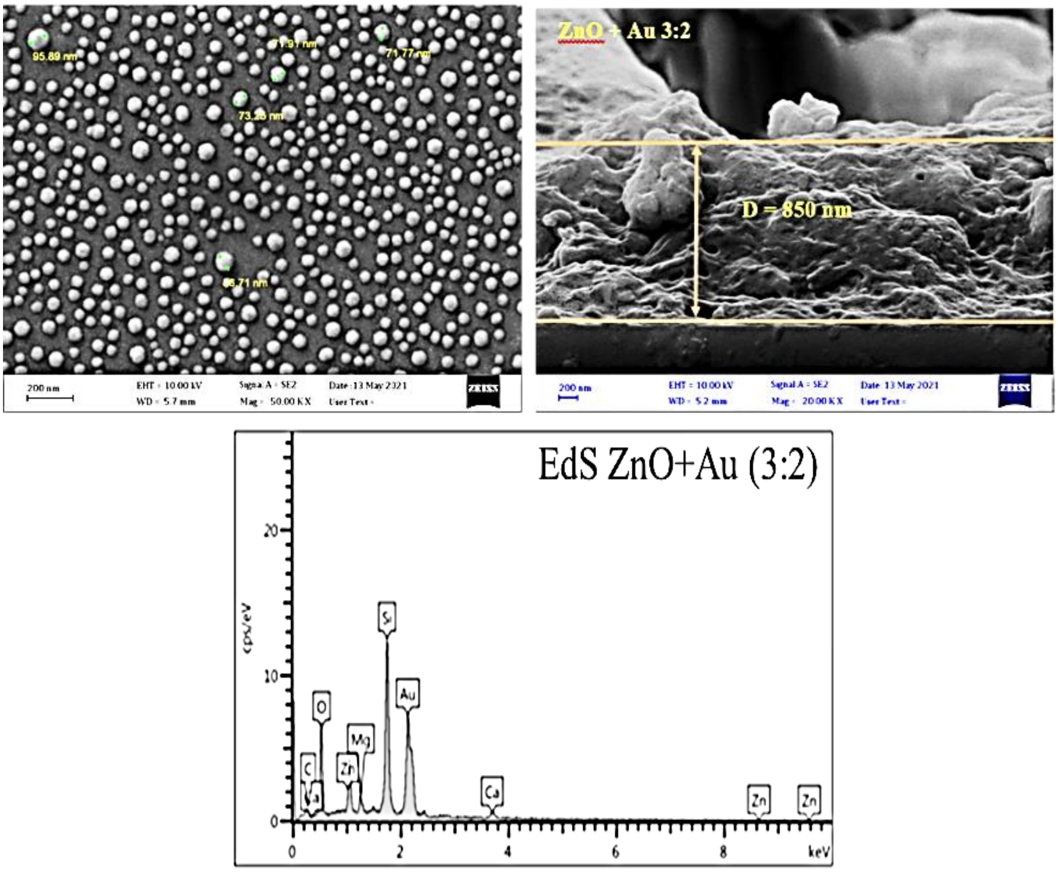

Fig. 3. FESEM images of (ZnO+Au) (3:2) thin film.

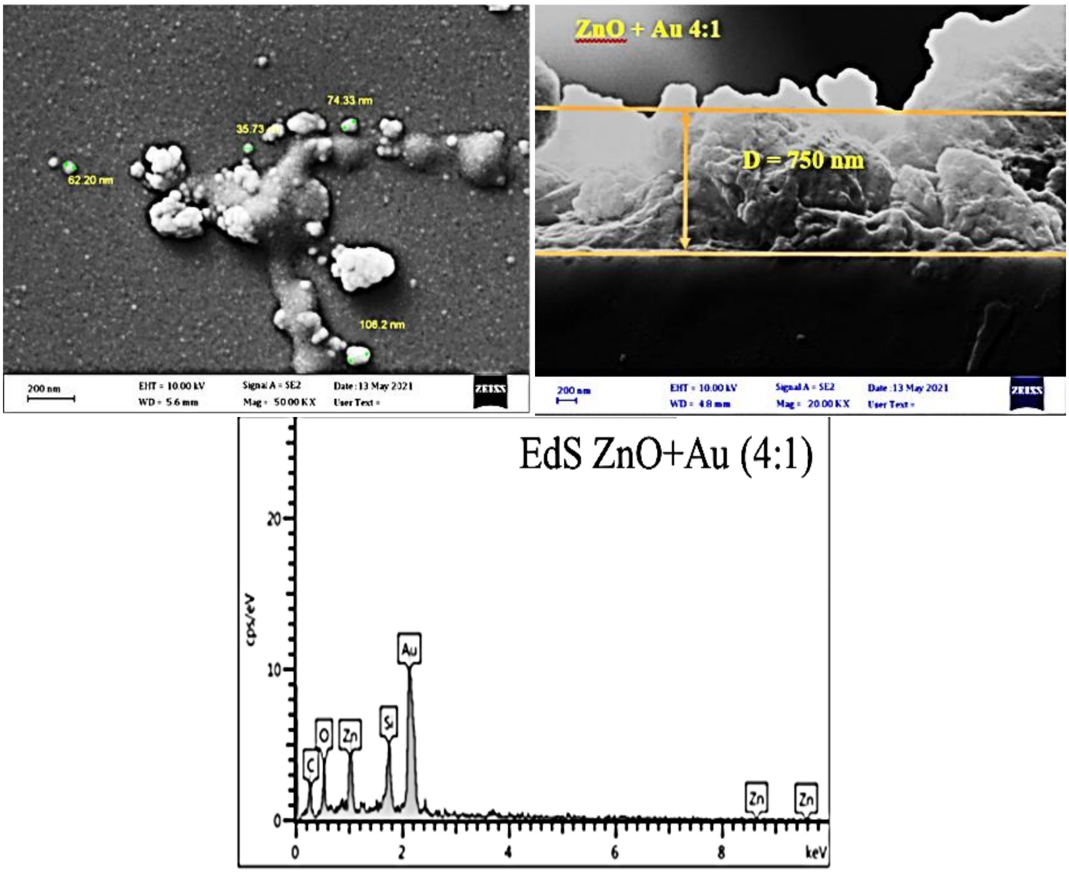

Fig. 4. FESEM images of (ZnO+Au) (4:1) thin film.

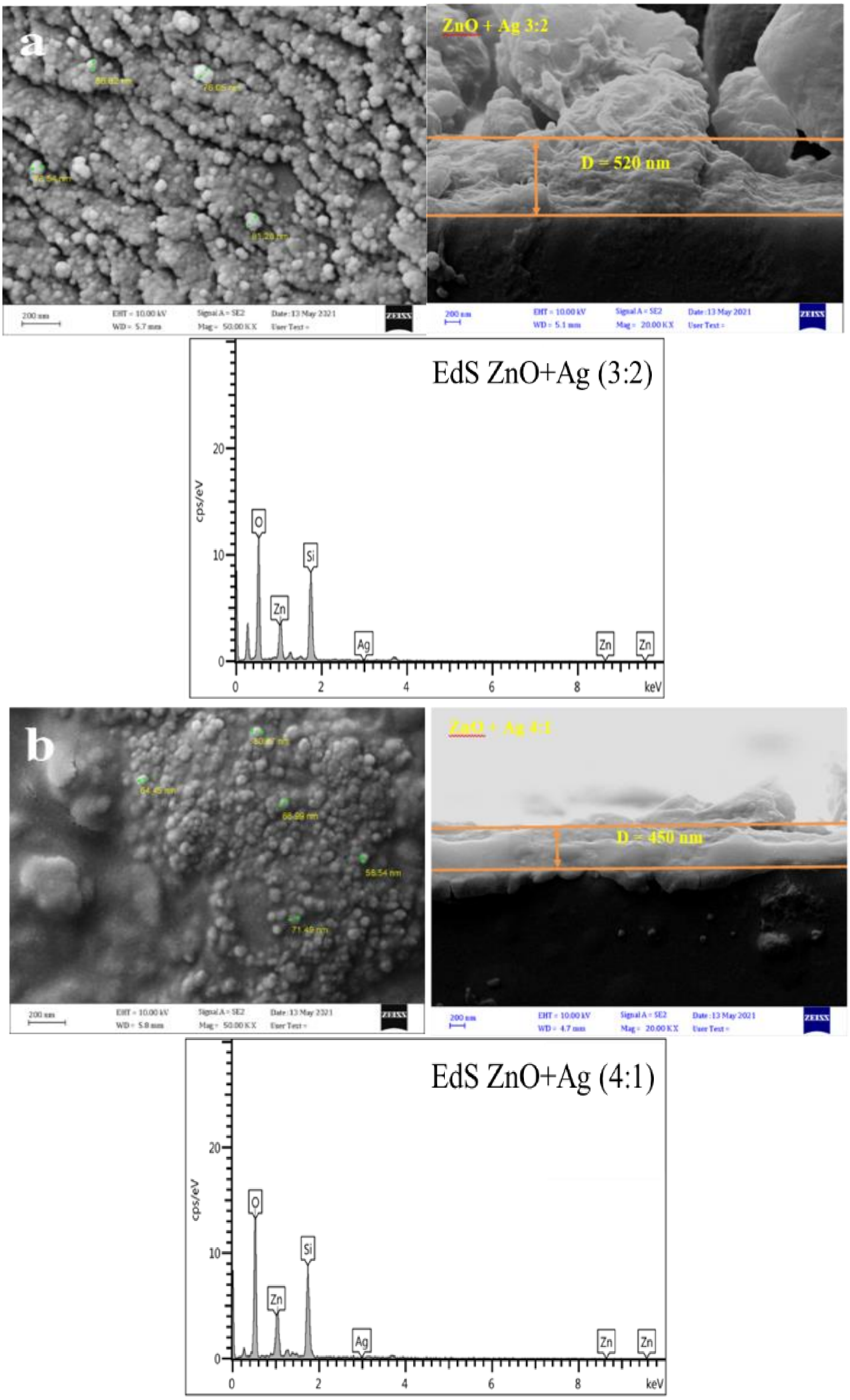

Fig. 5. FESEM images of a. (ZnO+Ag) (3:2) and b. (ZnO+Ag) (4:1) thin films.

3.1.2 X-ray Diffraction results of ZnO embedded with Au and Ag NPs

XRD patterns of ZnO (0.5 M) thin films deposited on quartz substrates using sol-gel spin coating method embedded with Au and Ag NPs were investigated by Low Angel X-Ray Diffraction and displayed in Figure (6). It can be noticed that the patterns exhibit six main diffraction peaks, three of them: (100), (002), and (101) belong to ZnO hexagonal phase with a wurtzite structure and the other peaks: (111), (200) and (220) belong to Au and Ag with cubic crystalline structure. All the diffraction peaks in the XRD patterns are in well agreement with JCPDS card numbers 36-1451 for ZnO, 04-0784 for Au, and 04-0783 for Ag [8, 17]. From the x-ray peaks positions and the presence many different diffraction peaks, it is concluded that the prepared films have polycrystalline structure. The patterns of the ZnO thin films embedded with Ag NPs also show the existence of another peak attributed to AgO phase corresponding to the orientations (111) identical to the standard pattern (JCPDS 03-5662). The strongest peaks occur at 2θ ~ (36.25°, 38.33°) are referred to (101) and (111) planes for ZnO and Au-Ag NPs. Also, the x-ray results revealed that the diffraction peaks intensity associated with Ag and Au increased as the amount of Au and Ag NPs increases.

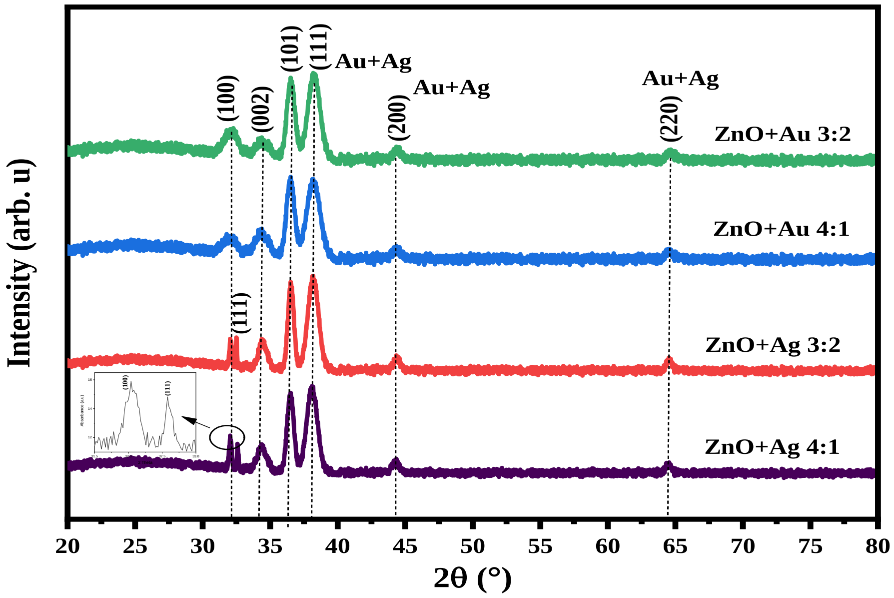

Fig. 6. XRD patterns of ZnO thin films embedded with Au and Ag NPs.

Crystallite size was calculated by using Scherrer’s equation:

$$D=(K\,\lambda)/(\beta\ \mathrm{Cos}\ \theta) \qquad (1)$$

where (D, λ, K, θ, and β) are the crystallite size, X-ray wavelength (1.54059 Å), a dimensionless shape factor (0.9), the Bragg’s angle, and the full width at half maximum (FWHM) of the selected peak, respectively [18].

The lattice constants have been found using the formula of hexagonal structure:

$$\frac{1}{d^2}=\frac{4}{3}\left[\frac{h^2+hk+k^2}{a^2}\right]+\frac{l^2}{c^2} \qquad (2)$$

where (d, a and c, and h, k, and l) are the interplanar distance, the lattice constants, and Miller indices, respectively [19].

All (d) values are given in tables (1 and 2). The lattice constants (a and c) for ZnO embedded with Au and Ag NPs as shown in tables (1 and 2) are in good agreement with the standard lattice constants of hexagonal structure (a = 3.2498 Å) and (c = 5.2066 Å). We can observe that the crystallite size increases with the increase of amount of Au and Ag NPs. The results are in agreement with other reports [19]. From the results, it was observed that the microstrain value decreases while the crystallite size increases.

Table 1. Structural parameters for ZnO+Ag (4:1) and (3:2).

Sample	2Θ (°)	FWHM (°)	D_{hkl} (nm)	Micro-strain $\times10^{-3}$	d-Spacing (Å)	Lattice Parameters (Å)
ZnO+Ag 4:1	32.0460	0.1574	52.5120	2.3914	2.7907	a = 3.222 c = 5.214
	32.5828	0.0984	84.1119	1.4690	2.7459	
	34.3651	0.5510	15.0915	7.7750	2.6074	
	36.4612	0.4723	17.7093	6.2566	2.4622	
	38.1363	0.5510	15.2549	6.9553	2.3578	
	44.3187	0.5510	15.5678	5.9032	2.0422	
	64.4263	0.3936	23.8557	2.7258	1.4450	
ZnO+Ag (3:2)	32.0811	0.1574	52.5166	2.3887	2.7877	a = 3.218 c = 5.208
	32.4947	0.0787	105.143	1.1783	2.7531	
	34.4071	0.5510	15.0932	7.7649	2.6044	
	36.7072	0.2558	32.7211	3.3643	2.4463	
	38.1303	0.5510	15.2547	6.9565	2.3582	
	44.3492	0.4723	18.1638	5.0562	2.0409	
	64.4790	0.4723	19.8864	3.2674	1.4439	

Table 2. Structural parameters for (ZnO+Au) (4:1) and (3:2).

Sample	2Θ (°)	FWHM (°)	D_{hkl} (nm)	Microstrain $\times10^{-3}$	d-Spacing	Lattice Parameters (Å)
ZnO+Au 4:1	32.4654	0.5510	15.0165	8.2576	2.7556	a= 3.18 c=5.230
	34.2593	0.9446	8.8006	13.3728	2.6153	
	36.6497	0.5117	16.3546	6.7412	2.4500	
	38.1390	0.2362	35.5866	2.9813	2.3577	
	44.3381	0.6298	13.6209	6.7442	2.0413	
	64.4149	0.3936	23.8542	2.7264	1.4452	
ZnO+Au 3:2	32.4324	0.6298	13.1366	9.4487	2.7583	a=3.185 c=5.231
	34.2548	0.9446	8.8004	13.3746	2.6156	
	36.7078	0.2165	38.6608	2.8473	2.4462	
	38.1402	0.2755	30.5103	3.4773	2.3576	
	44.4021	0.6298	13.6240	6.7334	2.0385	
	64.4505	0.3936	23.8589	2.7245	1.4445	

3.1.3. Raman spectroscopy studies

Figure 7a shows Raman spectra of ZnO thin films deposited on quartz substrate by spin coating technique. In low frequency region, one peak is observed at about 419 cm^{-1}. This peak is assigned to the two non-polar optical phonons (low frequency) modes of the sol-gel prepared ZnO films. The other peak at 561 cm^{-1} is attributed to the longitudinal optical (LO) mode of ZnO. The intensity of Raman peak varies with the oxidation of excess zinc in the ZnO film. This mode is created by the defects of O vacancies and Zn interstitials [20].

Figure 7b shows Raman spectra of ZnO thin films embedded with Au nanoparticles, where three typical peaks at Raman shift of 312 cm^{-1}, 453 cm^{-1}, 562 cm^{-1}, can be observed which are close to the previously reported results [21]. The shift in the absorption peak at Raman spectra indicated a strong interaction between ZnO and Au.

Raman spectra of ZnO thin films embedded with Ag NPs are shown in figure 7c. The three peaks observed at (420,560) cm^{-1} and 825 cm^{-1} are the vibration modes, the transverse optical (TO) and longitudinal optical (LO) polar branches appeared at about 420 cm^{-1} and 560 cm^{-1} respectively. The Raman peak located at 825 cm^{-1} could be assigned to the transverse optical (TO) and high frequency mode [22]. On embedding Ag in ZnO, the longitudinal optical peak broadened, the broadening in the phonon mode can be attributed to the scattering contributions of the longitudinal optical branch. The appearance of the peaks is attributed to the formation of oxygen vacancies, zinc interstitial defect states, and free carriers. Other three Raman peaks located at about 300, 649, and 742 cm^{-1} could be assigned to Raman spectra of Ag NPs embedded in ZnO nanostructures. The intensity of high phonon mode decreases indicating that the crystal quality of ZnO nanoparticles was degraded with increasing of Ag NPs. ZnO nanostructures exhibit a peak at 420 cm^{-1} which is due to the phonon mode of ZnO nanoparticles [22, 23].

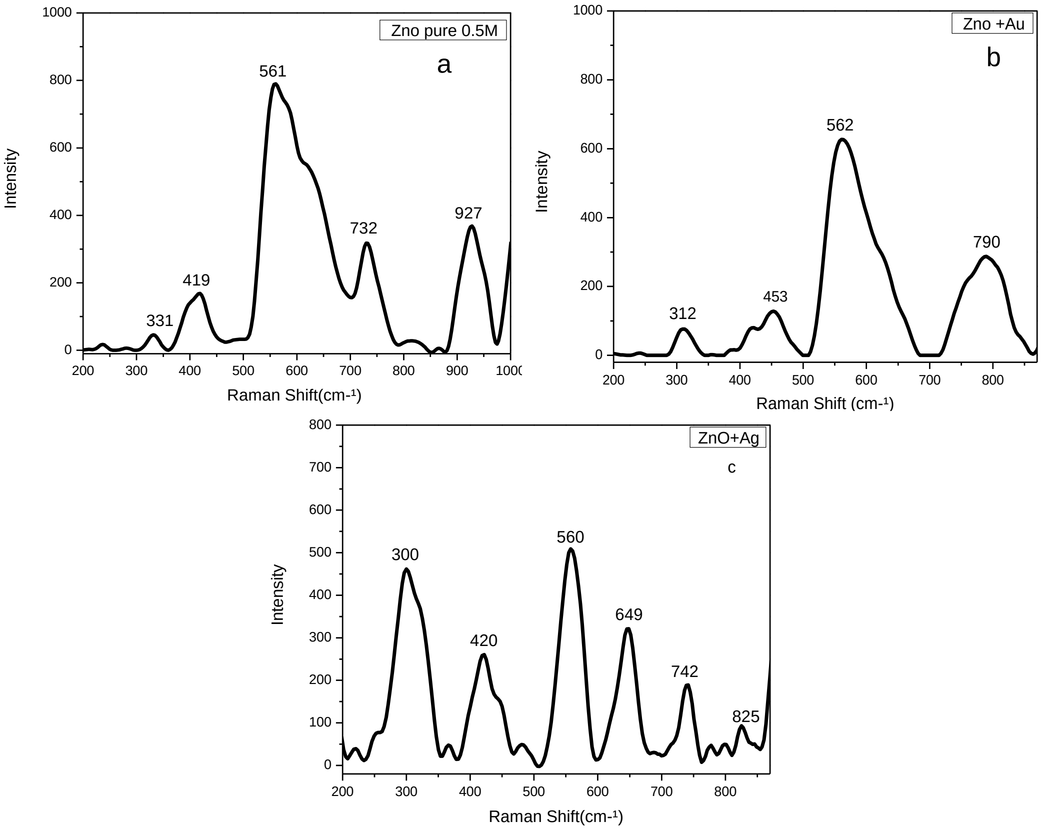

Fig. 7. Raman spectra of a. Pure ZnO, b. (ZnO+Au), and c. (ZnO+Ag) thin films.

4. Optical characterization

The optical measurement results include relations of the absorbance with wavelength for all samples.

4.1. Absorbance

Figure 8 shows the relationship between the absorbance (A) and wavelength in the range of 285-900 nm of ZnO thin films embedded with Au and Ag NPs.

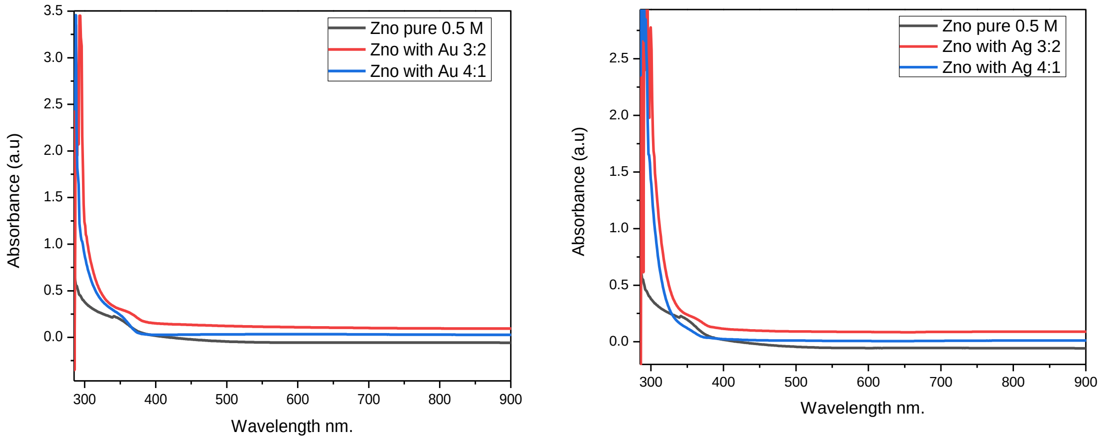

Fig. 8. Absorbance spectra of ZnO thin films embedded with Au and Ag NPs.

The absorbance values of all films decrease with the increase of wavelength. The strong UV absorption is observed in all the samples which show strong and sharp band at wavelength near 350 nm while the optical features in the visible range are ascribed to Au and Ag NPs. The absorbance increased with increasing the volumetric ratios of ZnO embedded with Au and Ag NPs. Moreover, at wavelengths above 500 nm, the absorption decreases and transmittance increases possibly due to the large scattering due to the presence of Au and Ag NPs [24,25]. In fact, a greater amount of metal embedded in the films leads to a larger optical extinction.

4.2. Optical Energy gap (Eg)

To obtain the optical energy gap of prepared thin films, a graph is plotted between photon energy and $(\alpha h\nu)^2$ as shown in figure 9. The optical energy gap was calculated by the Tauc's relation given by:

$$\alpha h\nu = A\,(h\nu - E_g)^r \qquad (3)$$

where (α, A, hν, E_g, and r) are the absorption coefficient, a constant, the photon energy, the optical energy gap, and the exponential modulus which depends on the type of material and the type of electronic transitions [25].

The values of optical energy gap (E_g) obtained are 3.45, 3.92, 3.90, 3.99 and 3.97, for pure ZnO, ZnO+Au (3:2), ZnO+Au (4:1), ZnO+Ag (3:2) and ZnO+Ag (4:1), respectively. We notice an increase in the value of energy gap with increasing the volumetric ratios of ZnO embedded with Au and Ag NPs.

The optical energy gap (E_g) of ZnO thin films embedded with Ag NPs is greater than ZnO thin films embedded with Au NPs. The optical band gap value of ZnO thin film in the current study agrees well with the previously reported values[25,26].

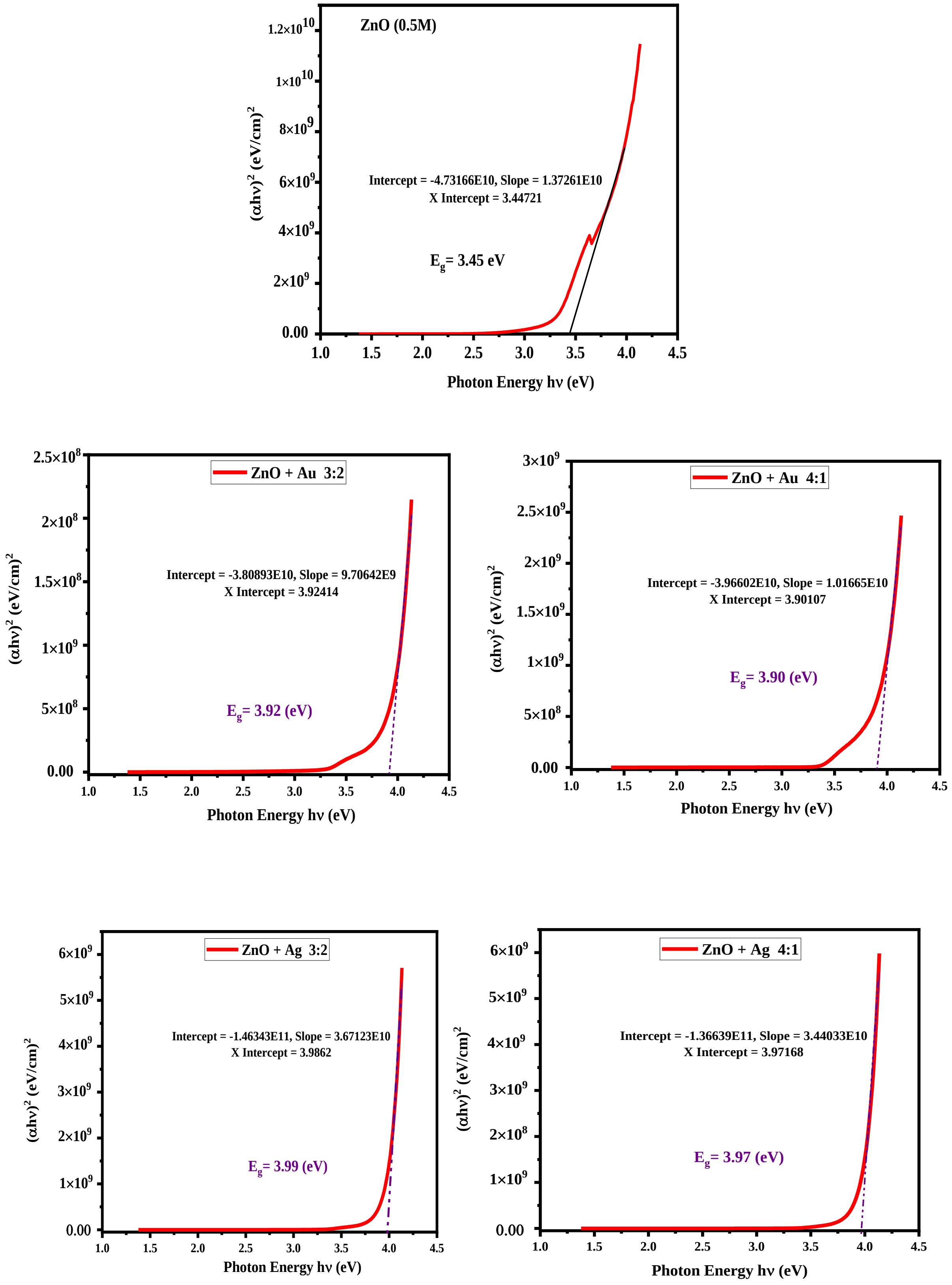

Fig. 9. Optical energy gap for ZnO thin films embedded with Au and Ag NPs.

5. Conclusions

Zinc Oxide thin films embedded with Au and Ag NPs were prepared by sol-gel spin coating method. The morphology, structure and optical properties of synthesized samples were investigated using a variety of measurements. FESEM shows an increase in the grain size of Au and Ag NPs embedded in ZnO. X-ray diffraction (XRD) patterns show hexagonal wurtzite structure and cubic crystalline structure which belong to ZnO and Au-Ag NPs respectively. A strong UV absorption was observed in all samples. Moreover, at longer wavelengths above 500 nm the absorbance decreases and transmittance increases. The Raman spectra of ZnO+Au thin films show three typical peaks at Raman shift of 312 cm^{-1}, 453 cm^{-1}, and 562 cm^{-1}. The shift in the absorption peak at Raman spectra indicated a strong interaction between ZnO and Au NPs. The Raman spectra of ZnO+Ag thin films exhibited three peaks at (420, 560) cm^{-1} and 825 cm^{-1} attributed to the vibration modes, transverse optical (TO) and longitudinal optical (LO) polar branches appeared at about 420 cm^{-1} and 560 cm^{-1} respectively. Transverse optical (TO) high frequency mode is located at 825 cm^{-1}. The optical band gap energy values increased with increasing the volumetric ratios of ZnO embedded with Au and Ag NPs.

The optical energy gap (E_g) of ZnO thin films embedded with Ag NPs is greater than ZnO thin films embedded with Au NPs. The optical band gap value of ZnO thin film in the current study agrees well with the previously reported values.

References

[1] E. R. Rwenyagila, B. A. Tuffour, MGZ. Kana and O. Akin-Ojo, J Mater Res; 29:2912, (2014); https://doi.org/10.1557/jmr.2014.298

[2] K. Sivarama Krishnan and T. L. Alford, Appl. Phys. Lett; 96:201109, (2010); https://doi.org/10.1063/1.3435467

[3] M. F. Al-Kuhaili, M. A. Al-Maghrabi, S. M. A. Durrani and I. A. Bakhtiari, J. Phys D Appl. Phys; 41:215302, (2008); https://doi.org/10.1088/0022-3727/41/21/215302

[4] M. Çopuroglu, L. H. K. Koh, S. O'Brien and G. M. Crean, J Sol-Gel Sci Technol; 52:432, (2009); https://doi.org/10.1007/s10971-009-2016-0

[5] D. C. Look, Mater Sci Eng, B; Vol. 80, Issues 1-3, 383-387 (2001); https://doi.org/10.1016/S0921-5107(00)00604-8

[6] L. Spanhel and M. A. Anderson, J. Am. Chem. Soc., 113, 8, 2826-2833 (1991); https://doi.org/10.1021/ja00008a004

[7] Z. L. Wang, J. Phys. Condens. Matter, 16, R829-R858, (2004); https://doi.org/10.1088/0953-8984/16/25/R01

[8] S. Wang, F. Jia, X. Wang, L. Hu, Y. Sun, G. Yin, T. Zhou, Z. Feng, P. Kumar and B. Liu, ACS Omega , 5, 10, 5209-5218 (2020); https://doi.org/10.1021/acsomega.9b04243

[9] D. B Chithrani, S. Jelveh , F. Jalali and M .v. Prooijen, Radiat. Res. 173, 719-728, (2010); https://doi.org/10.1667/RR1984.1

[10] J. F. Hainfeld, D. N. Slatkin, T. M. Focella and H. M. Smilowitz, Brit. J. Radiol., 79, 248-253, (2006); https://doi.org/10.1259/bjr/13169882

[11] E. J. Guidelli, A. Kinoshita, A. Ramos and O. Baffa, J. Nanopart. Res. 15, 1-9, (2013); https://doi.org/10.1007/s11051-013-1536-2

[12] E. J. Guidelli and O. Baffa, Med. Phys. 41, 32101, (2014); https://doi.org/10.1118/1.4865809

[13] G. Yang, "laser ablation in liquids" Principles and Applications in the Preparation of Nanomaterials", Pan-Stanford Publishing, Singapore, 1st edition (2012); https://doi.org/10.1201/b11623

[14] G. Amokrane, C. Falentin-Daudré, S. Ramtani and V. Migonney, Elsevier , IRBM 39, 268-278, (2018); https://doi.org/10.1016/j.irbm.2018.07.002

[15] P. Fageria, S. Gangopadhyay and S. Pande, RSC Adv, 4, 24962-24972, (2014);

https://doi.org/10.1039/C4RA03158J

[16] R. Khan, J. H. Yun, K. B. Bae, I. H. Lee, Journal of Alloy and Compounds, 682, 643-646, (2016); https://doi.org/10.1016/j.jallcom.2016.05.036

[17] C. Mondal, J. Pal, M. Ganguly, A. Kumar Sinha, J. Jana and T. Pal Article in New Journal of Chemistry, (2014); https://doi.org/10.1039/c4nj00227j

[18] Z. T. Khodair, N. A. Bakr, A. M. Hassan, A. A. Kamil, "Influence of substrate temperature and thickness on structural and optical properties of CZTS nanostructures thin films" Journal of Ovonic Research, Vol. 15, No. 6, 377 - 385, (2019).

[19] D. Aryanto, W. N. Jannah, Masturi, T. Sudiro, A. S. Wismogroho, P. Sebayang, Sugianto and P. Marwoto, Journal of Physics: Conf. Ser:Vol.817, 012025, (2017); https://doi.org/10.1088/1742-6596/817/1/012025

[20] R. Mahendran, M. Kashif, M. Saroja, M. Venkatachalam, T. Siva Kumar, A. Ayeshamariam, C. Sanjeeviraja and U. ashim, "Structural and optical characterization of ZnO thin films annealed at different temperatures", Journal of Applied Sciences Research, 9(9): 5460-5467, (2013).

[21] E. Budianto, Y. Yulizar1, I. S. Saputra, and S. Sudirman, AIP Conference Proceedings, 2349, 020006, (2021); https://doi.org/10.1063/5.0051749

[22] R. Sánchez Zeferino, M. Barboza Flores and U. Pal, Journal of Applied physics, 109, 014308, (2011); https://doi.org/10.1063/1.3530631

[23] A. Muravitskaya, A. Rumyantseva, S. Kostcheev, V. Dzhagan, O. Stroyuk and P. Michel Adam, Article in Optics Express, (2016); https://doi.org/10.1364/OE.24.00A168

[24] E. D. Gaspera, M. Guglielmia, A. Martucci , L. Giancaterini , C. Cantalini, Sensors and Actuators B, 164, 54- 63, (2012); https://doi.org/10.1016/j.snb.2012.01.062

[25] M. I. Khan, K.A. Bhatti, R. Qindeel, N. Alonizan and H. Saeed Althobaiti, Results in Physics, 7, 651-655 (2017); https://doi.org/10.1016/j.rinp.2016.12.029

[26] D . D Mulmi, A. Dhakal and B . R. Shah, Nepal Journal of Science and Technology Vol. 15, No.2,111-116(2014), https://doi:10.3126/njst.v15i2.12126